J. COMBIN. MATH. COMBIN. COMPUT. 127b (2025) 6203--6218

Journal of Combinatorial Mathematics and Combinatorial Computing
www.combinatorialpress.com/jcmcc

Combinatorial Press

Heat conduction analysis and performance prediction of metallurgical materials based on finite element method

Hongye He[1], Shubao Wang[1,✉], Junli Yu[1], Wenhui Liu[1]

[1] Qian'an College, North China University of Science and Technology, Qian'an, Hebei, 064400, China

ABSTRACT

In this paper, finite element simulation of heat transfer process is carried out using Cu composites reinforced with TiB2 of different particle sizes. Based on the FEA data, the BP neural network algorithm is integrated and optimized by the MEA algorithm to establish the FEA-MEA-BP performance prediction model. The results of thermal conductivity analysis show that the correction factor of the simulated thermal conductivity value of TiB2/Cu composites can be calculated using the finite element method as 2.3. Compared with the actual value measured by the LINSEISLFA1600 laser thermal conductivity meter, the fluctuation of the simulated thermal conductivity results from the experimental results is no more than 10% between 50~200°C, and the simulation performance has a high degree of accuracy. Taking 304L stainless steel as a sample, the RMSE, MAE and R^2 are improved to different degrees compared with other models, so the performance of the FEA-MEA-BP model is excellent in terms of the accuracy of prediction.

Keywords: finite element, BP neural network, MEA algorithm, heat transfer, FEA-MEA-BP

1. Introduction

As an important engineering material, metallurgical materials play a key role in industrial production. With the progress of science and technology and changes in demand, the research and development of metallurgical materials has been developed under the background of the "two-carbon" strategy and has been used in aerospace, energy, nuclear industry, automotive and other industries [1-2]. Traditional metallurgical materials are mainly metal materials, such as iron, aluminum, magnesium, copper and so on. These materials have good electrical conductivity, thermal conductivity and mechanical properties, and are widely used in industrial production, such as aluminum alloy is used in aviation, aerospace and other high-tech fields [3-5]. And advanced metallurgical materials are new types of metal materials, such as high-performance alloys, wear-resistant materials, high-temperature materials, etc., which have better performance and a wider range of applications. For example, high-

✉ Corresponding author.
E-mail address: 18232566700@163.com (S. Wang).
Received 25 February 2024; Revised 05 April 2024; Accepted 15 December 2024; Published Online 16 April 2025.
DOI: 10.61091/jcmcc127b-340

performance alloys with high strength, heat resistance and corrosion resistance are used in aerospace, energy and other high-end fields [6-7]. High-temperature materials such as ceramic materials and refractory materials are used in high-temperature furnaces, aerospace, nuclear industry and other fields because of their ability to maintain good performance in high-temperature environments [8-9]. And thermal conductivity properties are one of the key indicators to evaluate the performance of composite materials. The thermal conductivity of these materials affects the efficiency and speed of heat transfer, and its good or bad directly affects the use of the material and performance stability, which has become a key factor in restricting the manufacture of high-end precision equipment [10-11]. For many engineering and scientific applications, it is very important to understand and control the thermal conductivity of materials. Taking the metallurgical materials in aerospace as an example, the working temperature of aerospace engines is generally as high as 1000 degrees Celsius or more, if the thermal conductivity of the material is poor, the local heat aggregation, the material is prone to soften and creep, thus weakening its mechanical properties, material failure, affecting its structural integrity and functionality, which may result in serious safety accidents [12-15].

The finite element method is a numerical computational method for solving physical problems with complex structures. It can approximate the behavior of a physical system by partitioning it into many small finite elements and solving the response of the system based on the relationships between the elements and the physical equations [16]. The finite element method has a wide range of applications covering many engineering fields. In structural analysis, the finite element method is used to analyze and optimize the structural mechanical properties and thermal conduction analysis of buildings, aerospace vehicles, mechanical equipment, etc., by discretizing the structure into a finite number of elements, calculating the stress, strain, and displacement and deformation of the entire structure of each element, or by modeling the thermal conductivity coefficient and boundary conditions of the material to predict the temperature distribution, heat flux and other related parameters [17-20].

In this paper, TiB2/Cu composites with different particle sizes prepared by metallurgical method are taken as the object of study, and the heat conduction properties of TiB2 reinforced Cu-based composites with different particle sizes and at different temperatures are simulated using finite element analysis. The TiB2/Cu composites at different temperatures were also tested using a LINSEISLFA1600 laser thermal conductivity meter and compared with the finite element simulation results with a view to exploring the usability of finite element thermal conduction analysis. The finite element analysis theory is incorporated into artificial neural network and optimized by MEA algorithm MEA to establish FEA-MEA-BP metallurgical material property prediction model to predict the rheological stress and dynamic recrystallization volume, Euler angle, and shear stress of 304L stainless steel, and analyze the prediction accuracy of the model.

2. Establishment of finite element model for heat conduction of metallurgical composite materials

2.1. *Introduction to Finite Element Analysis Techniques*

The finite element analysis technique, in essence, is also a process of simulating real physical systems by means of a certain mathematical approximation [21]. With the help of simple models, interconnected elements and a fixed number of unknowns, the corresponding wireless unknown system is reduced. Finite element analysis method can decompose a complex problem into several simple small problems, and according to the small problems related to the speculation, the answer, to obtain the conditions required for the solution of this unknown, can provide more accurate data to the mechanical design, but also greatly improve the speed of mechanical design.

Finite element, is also a series of scattered, continuous units to reconstruct. Through the finite element analysis technology can realize the smallest sub-domain to solve. In the past, in the process of solving the overall definition of the domain, the use of traditional solution methods often need to fully comply with the overall definition of the domain requirements, which also results in significantly more difficult to solve, and the solution process is more prone to errors. The accuracy of the traditional solving method is still unsatisfactory in both the subdomain and the overall definition domain. By using the finite element analysis technique in solving the sub-domain, the closest data to the real situation can be obtained, and after solving each small unit, the conditions that conform to the overall definition of the domain can be deduced, thus significantly improving the accuracy of the calculation process. In the design of metallurgical machinery to use finite element analysis technology, in essence, is also a function to solve the simple sub-domain, the solution process for the overall definition of the domain of the relevant requirements do not need to pay attention to the process, which greatly enhances the convenience and accuracy of the solution process, which is also the biggest difference with the traditional solution methods.

The complex structure of composite materials exhibits a high degree of non-uniformity and anisotropy, which makes it difficult to predict the thermal response mechanism and heat conduction process of the materials. In the past decades of research, finite element analysis of heat transfer properties of composites is mainly based on multiscale methods. The aim of this paper is to establish a geometrical model of the composite material with the same size as the test specimen of the laser flash method by the computer-aided engineering software CATIA (version VR-R^{2}0). And the heat conduction analysis is carried out in the professional finite element analysis software ABAQUS (6.14) to investigate the heat conduction and thermal response process of the composite material under different prefabricated parts structural parameters. The finite element simulation process of heat conduction in this paper is shown in Figure 1.

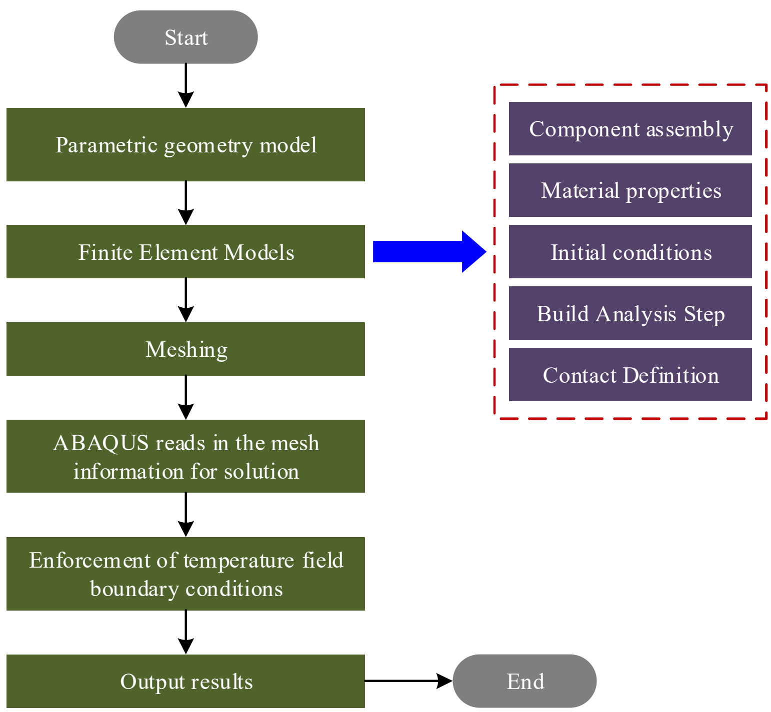

Fig. 1. Heat conduction finite element simulation process

2.2. Heat transfer mechanism

2.2.1. Basic Laws of Heat Transfer. According to Fourier's law, a fundamental law in heat transfer, the thermal conductivity of anisotropic materials depends on the direction of conduction [22]. Therefore, a more general form of the formulation of the anisotropic heat transfer equation states that the heat flux vectors in each direction depend on the temperature gradients in the three directions. For example, for the x direction:

$$q_x = -\lambda_{11}\frac{\partial T}{\partial x} - \lambda_{12}\frac{\partial T}{\partial y} - \lambda_{13}\frac{\partial T}{\partial z} \tag{1}$$

For directions x, y, and $z(x_i)$, this can be written as:

$$q_{x_i} = -\lambda_{i1}\frac{\partial T}{\partial \mathrm{x}} - \lambda_{i2}\frac{\partial T}{\partial y} - \lambda_{i3}\frac{\partial T}{\partial z} \tag{2}$$

Or abbreviated as:

$$q_{x_i} = -\lambda_{ij}\frac{\partial T}{\partial x_i} \tag{3}$$

Eq. The summation is solved repeatedly according to the subscript j. The three heat transfer components in Eq. appear in each coordinate direction, and the heat transfer coefficient expression takes the following tensor form:

$$\lambda = \begin{bmatrix} \lambda_{11} & \lambda_{12} & \lambda_{13} \\ \lambda_{21} & \lambda_{22} & \lambda_{23} \\ \lambda_{31} & \lambda_{32} & \lambda_{33} \end{bmatrix} \tag{4}$$

When the coordinate system $x-y-z$ is rotated about the origin, a new coordinate system is obtained $x'-y'-z'$. The new heat transfer matrix λ' can be written as:

$$\lambda' = P^T \lambda P \tag{5}$$

where P is the direction cosine matrix:

$$P = \begin{bmatrix} \cos(x',x) & \cos(x',y) & \cos(x',z) \\ \cos(y',x) & \cos(y',y) & \cos(y',z) \\ \cos(z',x) & \cos(z',y) & \cos(z',z) \end{bmatrix} \tag{6}$$

Indeed, λ is a second-order tensor that can be transformed into a diagonal matrix form under the choice of an appropriate coordinate system. Therefore:

$$P^T \lambda P = \begin{bmatrix} \lambda_\zeta & 0 & 0 \\ 0 & \lambda_\eta & 0 \\ 0 & 0 & \lambda_\zeta \end{bmatrix} \tag{7}$$

And there is:

$$\left.\begin{aligned} q_\zeta &= -\lambda_\xi \frac{\partial T}{\partial \xi} \\ q_\eta &= -\lambda_\eta \frac{\partial T}{\partial \eta} \\ q_\zeta &= -\lambda_\zeta \frac{\partial T}{\partial \zeta} \end{aligned}\right\} \tag{8}$$

The negative sign "-" in the equation indicates the direction of heat flow in the direction of temperature decrease.

$\frac{\partial T}{\partial \xi}$, $\frac{\partial T}{\partial \eta}$, $\frac{\partial T}{\partial \zeta}$ is the temperature gradient in the (ξ,η,ζ) direction, $K \cdot m^{-1}$.

q_ξ, q_η, q_ζ is the heat flow density in the (ξ,η,ζ) direction, $W \cdot m^{-2}$.

(ξ,η,ζ) is the principal axis of the heat conduction equation in the coordinate system.

λ_ξ, λ_η, and λ_ζ are the principal thermal conductivities $\left(W\cdot m^{-1}\cdot K^{-1}\right)$. If $\left(\xi,\eta,\zeta\right)$ are mutually perpendicular axes, then the material is orthogonally anisotropic. In this case, $\lambda_{ij}=0(i\neq j)$, $\lambda_{ii}=\lambda_i$ of the λ matrix, i.e., the non-diagonal entries in the matrix are all zero, while the main diagonal entries have different values, representing the thermal conductivity of the material in different directions, respectively. For isotropic materials, $\lambda_{ij}=0(i\neq j)$, $\lambda_{ii}=\lambda$, i.e., the non-diagonal terms are all zero, while the main diagonal terms all have the same value.

In addition, the so-called heat flow density above refers to the amount of heat per unit area that flows over one side of the surface of the material in a unit of time. For a single-cell model of a composite material, the temperature gradients $\frac{\partial T}{\partial\xi}$, $\frac{\partial T}{\partial\eta}$, $\frac{\partial T}{\partial\zeta}$ and the average heat flow at the boundary q_ξ, q_η, q_ζ are:

$$q_i=\frac{Q_i}{A_i}\ And\ \frac{\partial T-\Delta T}{\partial i}L_i(i=\zeta,\eta,\zeta) \tag{9}$$

It can be seen that the thermal conductivity (also known as thermal conductivity) represents the heat flux of the material under stable heat transfer conditions and unit temperature gradient, the larger the value, the easier the material conducts heat, the better the heat transfer effect; on the contrary, the smaller the coefficient of thermal conductivity, the more difficult it is to conduct heat, and the better the material's adiabatic and thermal insulation performance. Therefore, it is of great significance to accurately obtain the thermal conductivity of a material in the basic research, analytical calculation and engineering design of heat transfer process.

2.2.2. Temperature field control equations. If the heat transfer conditions on the material boundary do not change with time, after a certain time of heat exchange, the temperature of the points inside the material will not change with time, and this type of heat transfer is called steady state heat transfer. The finite element analysis of steady state heat transfer based on composite materials can obtain the temperature and heat flow distribution of the material, for which the governing equations of the temperature field are derived [23].

In any object where heat conduction occurs, we can choose any micrometric parallel hexahedron inside its volume to push to the differential equation of heat conduction, let the side length of the micrometric body is dx, dy, dz. According to the energy balance it can be seen that the heat flow per unit length, per unit time in the direction of x, y, and z is denoted by q_x, q_y, and q_z, respectively, and the difference of the inflow and outflow of the heat in the unit is:

$$\begin{aligned}&dydz\left(q_x+\frac{\partial q_x}{\partial x}-q_x\right)+dxdz\left(q_y+\frac{\partial q_y}{\partial y}-q_y\right)\\&+dxdy\left(q_z+\frac{\partial q_z}{\partial z}-q_z\right)\end{aligned} \tag{10}$$

From the conservation of heat, the above equation is equal to the heat produced in the cell per unit of time $Qdxdydz$ plus the heat produced per unit of time due to the change in temperature $-\rho c\frac{\partial T}{\partial t}dxdydz$ (here c is the specific heat of the cell, ρ is the mass density of the cell, and $T(x,y,z,t)$ is the temperature distribution). From this, it can be derived:

$$\frac{\partial q_x}{\partial x}+\frac{\partial q_y}{\partial y}+\frac{\partial q_z}{\partial z}-Q+\rho c\frac{\partial T}{\partial t}=0 \tag{11}$$

From the relationship between heat flow and temperature in Fourier's law the above equation can be transformed into:

$$\lambda_{xx}\frac{\partial^2 T}{\partial x^2}+\lambda_{yy}\frac{\partial^2 T}{\partial y^2}+\lambda_{zz}\frac{\partial^2 T}{\partial z^2}+Q-\rho c\frac{\partial T}{\partial t}=0 \tag{12}$$

Where T represents the temperature, λ_{xx}, λ_{yy}, λ_{zz} is the thermal conductivity of the material. For isotropic materials, $\lambda_{xx}=\lambda_{yy}=\lambda_{zz}$ the above equation can be simplified to:

$$\lambda\left(\frac{\partial^2 T}{\partial x^2}+\frac{\partial^2 T}{\partial y^2}+\frac{\partial^2 T}{\partial z^2}\right)+Q-\rho c\frac{\partial T}{\partial t}=0 \tag{13}$$

where λ is the thermal conductivity of the isotropic material.

When the material under consideration is a steady state heat conduction problem with no internal heat source, Eq. (14) can be simplified as:

$$\lambda_{xx}\frac{\partial^2 T}{\partial x^2}+\lambda_{yy}\frac{\partial^2 T}{\partial y^2}+\lambda_{zz}\frac{\partial^2 T}{\partial z^2}=0 \tag{14}$$

And for the usual anisotropic case, the heat conduction equation can be expressed in the right-angled coordinate system as:

$$\begin{aligned}&\lambda_{xx}\frac{\partial^2 T}{\partial x^2}+\lambda_{yy}\frac{\partial^2 T}{\partial y^2}+\lambda_{zz}\frac{\partial^2 T}{\partial z^2}+\left(\lambda_{xy}+\lambda_{yx}\right)\frac{\partial^2 T}{\partial x\partial y}\\&+\left(\lambda_{xz}+\lambda_{zx}\right)\frac{\partial^2 T}{\partial x\partial z}+\left(\lambda_{yz}+\lambda_{zy}\right)\frac{\partial^2 T}{\partial y\partial z}=0\end{aligned} \tag{15}$$

From the above discussion, it is clear that the differential equation for heat transfer is an equation in the form of a mathematical expression describing the temperature distribution within a heat conducting material for thermal conductivity phenomena with different characteristics. For a particular thermal conductivity phenomenon, the corresponding initial and boundary conditions must be given when solving for the temperature field distribution inside the material.

Usually there are two main types of boundary conditions:

The first is that the magnitude of the temperature is specifically determined, and this value may be a fixed value or a quantity that varies with time as a function of time, and this type of boundary condition is called a Dirichlet boundary condition or a fundamental boundary condition. The second type of boundary condition is where the normal heat flux at the boundary is known, and this type of boundary condition is often referred to as the Neumannn boundary condition or the natural boundary condition, which has the expression (16):

$$\begin{aligned}&T=T_0(x,y,z,t)\\&\bar{q}=-\lambda\frac{\partial r}{\partial n}\end{aligned} \tag{16}$$

3. MEA-BP-FEA performance prediction modeling

With the development of materials science and artificial intelligence technologies, data-driven materials research methods have become a new paradigm to revolutionize the traditional trial-and-error approach. Although machine learning strategies have been widely used in materials research, their physical interpretability is low. In order to take into account the superiority of machine learning prediction, this section proposes a finite element-based guided machine learning approach for prediction modeling. This approach combines the mechanisms of numerical computational methods of finite element analysis (FEA) and aims to provide a deeper understanding of the crystal plastic deformation process of metallurgical materials. However, it also faces the problems of cumbersome finite element modeling process and long computation time when the model is more complex.

Considering that most of the actual materials have polycrystalline structures, researchers have used the crystal plasticity finite element simulation method to deeply investigate the changes in the plastic deformation process and the evolution of grain orientation information in the mesoscopic state. Some of these recent studies have combined crystal plasticity with machine learning algorithms to develop more reliable simulation predictions.

The finite element completion of the intrinsic model usually goes through two processes: first, the corresponding stress increment and inelastic (plastic) strain increment are calculated according to the appropriate integration method using the strain increment derivation provided by Abaqus, and then the values of the here-and-now stress-strain state are updated again by using this as the initial strain increment: then, at the end of the stress-strain updating, the corresponding coherent tangent modulus is calculated and applied to the implicit solver Standard of Abaqus, which ensures convergence and speed in the computation of the program.

The BP neural network algorithm is a well-known multi-layer feed-forward network that stores and learns a large number of mathematical relationships between inputs and outputs [24]. The BP neural network model usually consists of an input layer, an implicit layer and an output layer. The classical BP algorithm consists of two processes: forward propagation of the signal and backward propagation of the error, and the two processes alternate with each other to obtain the weighting vector and the threshold value, thus minimizing the error function of the network. Since the BP neural network algorithm is based on the fastest descent method for solving, it has low computational cost and rapid processing, and can mimic the human mind to reason and analyze the mechanism.

n is the number of samples and the output vector of the network is:

$$Y = \left[y_1, y_2, \cdots, y_n \right]^T \tag{17}$$

However, the BP algorithm has a weak global search ability and a slow convergence speed. It needs to be combined with other algorithms to improve the global search ability, so as to improve the accuracy and stability of energy consumption prediction.

Thought evolution algorithms evolved inspired by genetic algorithms and follow some of the concepts of genetic algorithms (e.g., environment, population, and individuals, etc.). The evolutionary algorithm of thinking is mainly composed of populations, subpopulations, individuals, and bulletin boards, and proposes "convergence" and "alienation" to replace the two ideas of "crossover" and "variation" in genetic algorithms [25]. The computational steps of the MEA algorithm are as follows:

Step1 Generate a certain number of individuals randomly in the whole solution space, and determine the M winning individuals with high scores and the T temporary individuals by comparing the scores between them (applicability function $\xi_{i,j}$):

$$\xi_{i,j} = \sqrt{\frac{a}{\sum_{z=1}^{a} \left(g_{i,j,z} - p_{i,j,z} \right)^2}} \tag{18}$$

Where: $p_{i,j,z}$ is the data corresponding to the individual $N_{i,j}$ collected by the detector; $g_{i,j,z}$ is the target value for training; a is the length of the detector data.

Step2 Taking these individuals as the center, the individuals within a certain range around them form the winning population, and the remaining individuals form the temporary population.

Step3 In the "convergence" step, the individuals of local sub-population S_i in each population are struggled to obtain the local optimal individual $N_{i,nb}$, and in the iterative process, when the optimal individual no longer changes, the sub-population is considered to be mature, and the score of the optimal individual x in the sub-population is taken as the score of the sub-population; Individuals N_i of subpopulation S_i obeyed a normal distribution:

$$N_i \left(\mu_i, C_i \right) \tag{19}$$

Where: μ_i is the coordinates of the optimal individual $N_{i,nb}$, i.e., the connection weights and thresholds of the neural network; C_i is the covariance matrix, which can be denoted as $C_i = diag\left(\sigma_1, \sigma_2, \cdots, \sigma_m, \cdots, \sigma_{K-1}, \sigma_K\right)$. After p iterations, the diagonal element in C_i can be denoted as $C_i = diag\left(\sigma_1^p, \sigma_2^p, \cdots, \sigma_m^p, \cdots, \sigma_{k-1}^p, \sigma_\kappa^p\right)$. For the initial value $\sigma_m^0 (m = 1, 2, \cdots, K)$ can be denoted as:

$$\sigma_m^0 = \frac{H_m - L_m}{10} \tag{20}$$

where: H_m is the upper limit in dimension m; L_m is the lower limit in dimension m. The individual variance in the next iteration can be expressed as:

$$\sigma_m^{n+1} = \gamma_1^n \sigma_m^n + \gamma_2^n \sigma_m^n \tag{21}$$

Where: γ_1^n and γ_2^n are random numbers with values in the range of $[0.1, 0.5]$, and σ_m^n is the distance between the winning individuals of generation $n-1$ and generation n.

Step4 record the scores of each sub-population on the bulletin board, and carry out the "alienation" step in the whole world, that is, compare the scores of the winning sub-population and the temporary sub-population, retain the sub-population with the high score, and the other sub-population is released, and the individuals released in the solution space form a new temporary sub-population, so as to complete the replacement of the winning sub-population and the temporary sub-population.

Step5 Repeat Step3 and Step4 continuously until the optimal scores of all populations cannot be further improved or the number of global iterations reaches the upper limit, then the global optimal solution N_{nb} can be obtained, which will be used as the initial weights as well as the threshold value of the BP neural network, so as to shorten the training time of the neural network and improve the efficiency of optimization selection.

Before executing the MEA-BP algorithm, it is necessary to normalize all the data, due to the inconsistency of the unit of these data in the neural network, it is necessary to transform the sample data into a number between 0 and 1 through normalization, and then convert them back when all the data have completed the training of the neural network. The normalization equation is as follows:

$$x_k = \frac{x_k - x_{\min}}{x_{\max} - x_{\min}} \tag{22}$$

Where: $x_{\min}$ is the minimum value in the input vector; $x_{\max}$ is the maximum value in the input vector.

4. Heat transfer simulation and performance prediction by the finite element method

4.1. *Validation and analysis of finite element heat transfer simulation results*

4.1.1. Simulation results and analysis of thermal conductivity at different temperatures. To verify the finite element simulation results, TiB2/Cu composites with different particle sizes were prepared by powder metallurgy method in this paper. The total volume fraction of TiB2 particles is 5 vol%, and the particle sizes are 2 μm, 10 μm and 50 μm, respectively.The TiB2 particles are uniformly distributed in the Cu matrix, and the interfacial bonding is good and the organization is dense without obvious defects under the premise that neither wettability nor reaction occurs between the reinforcing body particles and the Cu matrix. The thermal conductivity of TiB2/Cu composites prepared with different particle sizes is examined, and the experimental results are compared and analyzed with the simulation results.

The simulated temperature distribution cloud and temperature gradient distribution of thermal conductivity of TiB2/Cu composites with TiB2 particle size of 2 μm at temperatures of 100°C, 200°C, and 280°C, respectively, are shown in Fig. 2. Using the finite element model, the simulated values of thermal conductivity of TiB2/Cu composites are obtained and the correction factor of 2.3 is chosen. It can be seen that the TiB2/Cu composite thermal conductivity simulation results are basically in agreement with the experimental results, and the thermal conductivity of the composite is in a small range of fluctuation state (the fluctuation range is not more than 10%) between 50 and 200 °C. After 200°C, both the simulated and experimental values show a trend of increasing with increasing temperature and are in good agreement.

At lower temperatures, composites are dominated by phonon thermal conductivity. The decisive factors for thermal conductivity in the lower temperature interval are: phonon heat capacity C, phonon mean velocity v and phonon mean free range l. Among them, the phonon mean velocity v can usually be regarded as a constant, and the phonon heat capacity is proportional to the temperature T. The value of l varies little at low temperatures, lying between the values of grain linearity and lattice spacing. The value of l does not vary much at low temperatures and lies between the values of grain linearity and lattice spacing. At the same time the presence of two binding interfaces between the grains and the substrate can have an effect on the phonon motion.

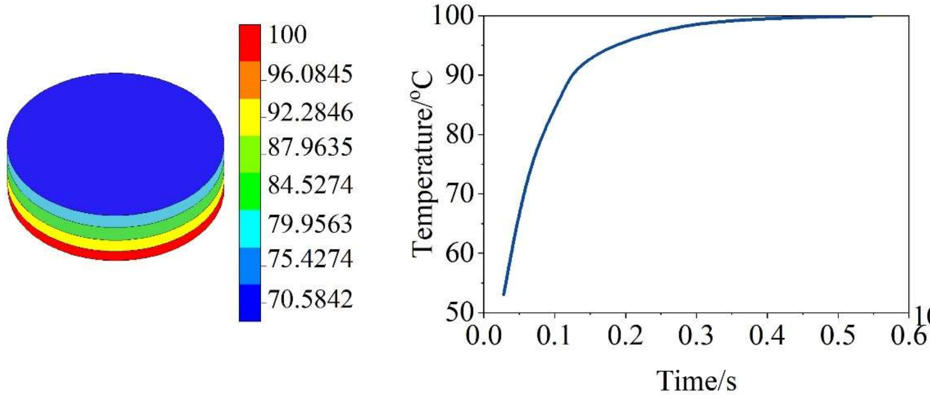

(a)100oC

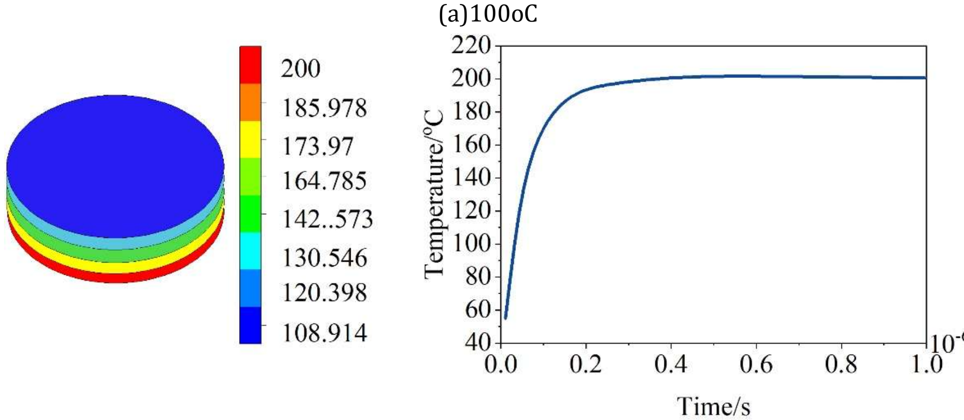

(b)200oC

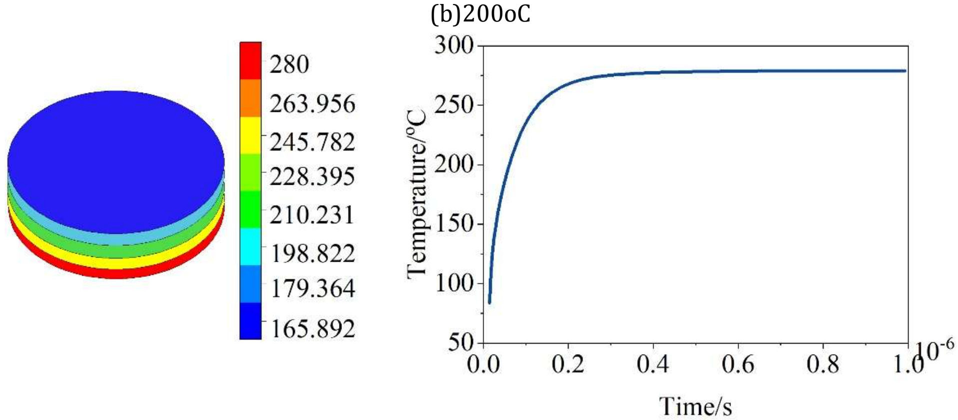

(c)280 oC

Fig. 2. Simulation results and temperature gradient profile

4.1.2. Simulation results and analysis of thermal conductivity of different particles. Comparison of the simulation results with the measurement results of the LINSEISLFA1600 laser thermal conductivity meter is shown in Fig. 3. The thermal conductivity of the composites fluctuates in a small range when the temperature is 50~200℃. This is due to the fact that the effect of different thermal expansion coefficients of the two phases at the interface is not considered in the simulation process, and the difference between the simulated value and the experimental value is relatively large, fluctuating within the range of 10%. As the temperature increases, the phonon mean free range l decreases and the heat capacity C remains proportional to the temperature. At this point, the increase in heat capacity C will have a greater effect compared to the decrease in mean free range l. After 200 °C the thermal conductivity shows a trend of increasing with temperature. The thermal conductivity curves of the composites overlap at 200 °C due to the change in the coefficient of thermal expansion reflecting the restraining effect of the reinforcement particles on the thermal expansion of the Cu matrix.

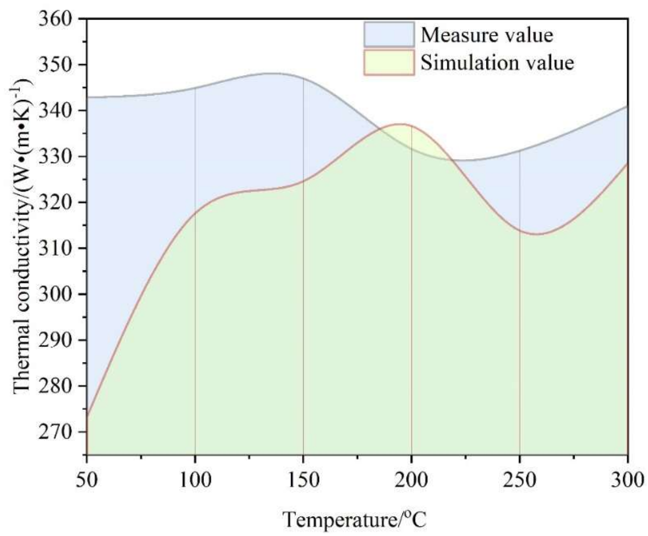

(a)2μm

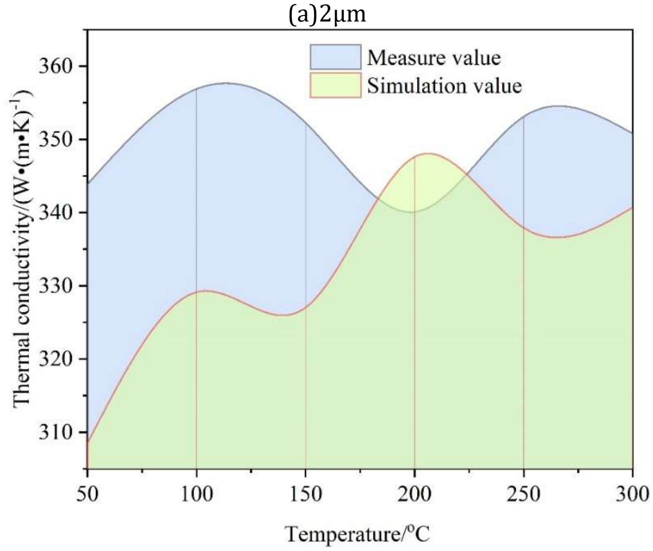

(b)10μm

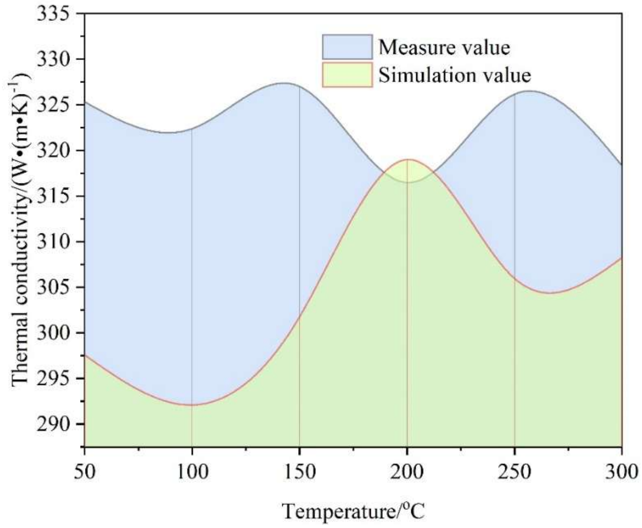

(c)50μm

Fig. 3. Thermal conductivity simulation value and experimental value

The relevant calculation results are shown in Table 1. It can be seen that both the interface stress value and the equivalent stress at the interface increase with the increase of temperature. When the equivalent stress value exceeds 60 MPa (the yield stress of Cu matrix), the Cu matrix composite will undergo plastic deformation. It can also be seen from the table that the equivalent stress value of TiB2/Cu composite will reach 66.4 MPa at 200°C, leading to plastic deformation. Due to the difference in the thermal expansion coefficients of the Cu matrix and TiB2 particles, plastic deformation of the Cu matrix will be induced when heated to 200 °C, resulting in considerable internal stresses. Some of these internal stresses exist in the form of tensile stresses on the reinforcement particles, increasing their surface area. From the phonon boundary scattering phenomenon, it can be seen that the collisions of phonons with the boundary of the reinforcement particles will be significantly increased, and the mean free range l of the phonons is thus reduced. The decrease of the mean free range l will cause the experimental value of thermal conductivity to show a decreasing trend at 200 °C. While the yield stress of Cu matrix is not considered in the simulation process, the simulated value of thermal conductivity will not show a decreasing trend at 200°C.

Table 1. The calculation of the equivalent stress of stress and interface

Temperature/oC	50	100	150	200	250	280
Interfacial stress/MPa	20.8	62.3	104.1	145.3	187.2	212.2
σe/MPa	9.4	28.2	47.6	66.4	84.7	95.2

4.2. Performance prediction study based on Finite Element Method (FEM)

4.2.1. Experimental materials and methods. In this study, 304L stainless steel cast ingot obtained by vacuum melting was used as the test material, and its chemical composition is shown in Table 2. Cylindrical specimens with a diameter of 10 mm and a length of 15 mm were machined from 304L stainless steel cast ingots by applying electric spark wire cutting (WEDM) technique and polished to a bright surface using water-resistant sandpaper. The thermal simulation compression test was carried out on the Gleeble-3800 thermal simulator at 900°C, 950°C, 1000°C, 1050°C, 1100°C and 1150°C, in order to effectively reduce the frictional resistance between the sample and the equipment, an appropriate amount of graphite was coated between the sample and the indenter as a lubricant, with a strain rate of 0.01, 0.1, 1 and 101s, and a deformation of 50%. The samples were water-cooled immediately after the test.

Table 2. The chemical composition of 1.52 % Cu-304L (wt%)

Sample	C	Si	Mn	P	S	Cr	Ni	Cu
304L	0.004	0.45	1.63	0.010	0.002	18.12	8.46	1.54

The accuracy of machine learning models is strongly influenced by the characteristics of the training dataset, and the construction of accurate models requires a dataset rich in sufficiently representative information. For this reason, the data generated from finite element simulations need to be carefully categorized to ensure that the number of features input to the model is minimal and sufficient to support accurate predictions. The process of selecting features from the available data and transforming them into machine learning models is known as “feature engineering”. The significance of the state variables is shown in Table 3.

In the training process of machine learning models, a large amount of data is needed to train and learn the machine learning model in order to achieve accurate prediction results, however, there are often problems such as large differences in the scale of the data sets used. Therefore, the sample dataset is normalized here to improve its prediction accuracy.

Table 3. The meaning of state variables

SDV	Variable meaning
1-12	Variable meaning
13-14	Current strength
25-36	Shear strain
37-72	Shear stress
73-108	Sliding vector
09-120	The direction of the slip direction cosine
121	Shear strain of each slip system
122-124	Shear strain of all slip lines
125	The number of each slip system
126-130	Rheological stress
131-135	Dynamic recrystalline integral number

4.2.2. Predictive performance analysis. In order to demonstrate the reliability of the method of fusing finite elements and machine learning, a comparison is made by comparing it with the unoptimized BP as well as the MEA-BP model without considering finite elements. In order to quantitatively evaluate the prediction performance of the proposed model, it was evaluated by introducing the mean square correlation coefficient (R^2), root mean square error (RMSE) and mean absolute error (MAE).The prediction performance indices of the three different prediction models are shown in Fig. 4, which clearly shows that the prediction performance of the MEA-BP-FEA model is better compared to BP and MEA-BP, with the rheological stresses and dynamic RMSE, MAE and R^2 for recrystallization volume fraction were 3.6284 MPa, 1.4526 MPa, 0.9942 and 0.0292 MPa, 0.0184 MPa, 0.9937, respectively. All of its evaluation indexes are significantly improved, proving that the machine learning prediction model guided by finite elements has excellent prediction accuracy.

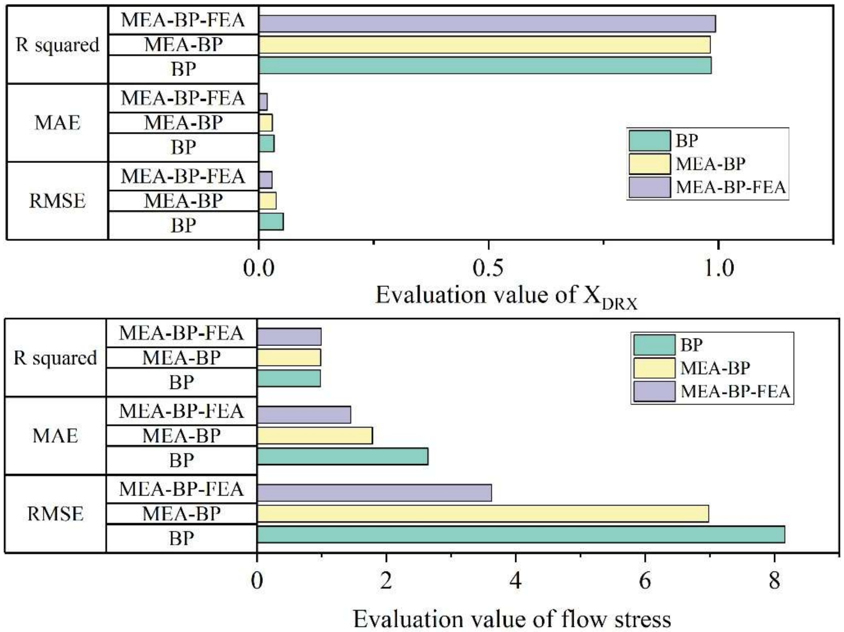

Fig. 4. The predictive energy indicators of three different predictive models

Through comparative screening, the feature parameters are selected to cover as many mesoscale responses as possible in the material. In this paper, the input features used to train the machine learning model are the shear stress of the crystal, the normal vector of the slip surface, and the direction cosine of the slip direction, and the output features are the evolved shear stress, the normal vector of the slip surface, and the direction cosine of the slip direction.

Comparison of experimental and predicted values is shown in Fig. 5, which shows that most of the predicted results of the MEA-BP model and the measured results are distributed on a 45-degree straight line, and a small part of the distribution of the location of a certain deviation. By evaluating the metrics, the predictive performance of the Euler angles in Fig. (a) has a R^2 of 0.9934, RMSE of 5.9368, and MAE of 3.6287, and the predictive performance of the shear strains in Fig. (b) has a R^2 of 0.9789, RMSE of 0.00822, and MAE of 0.0714. In terms of prediction accuracy, the finite element MEA-BP based neural network model still performs very well, thus proving that the neural network model is very adaptable and reliable for crystal level data prediction.

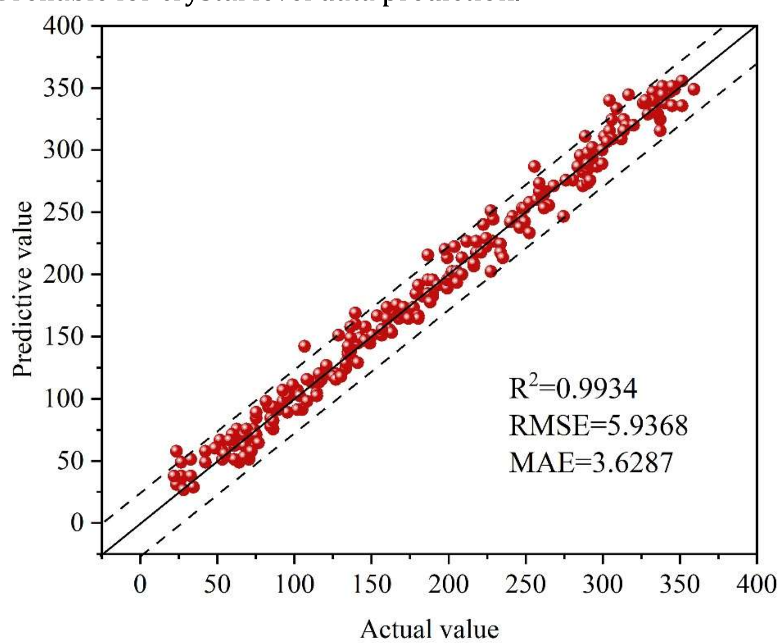

(a) euler Angle

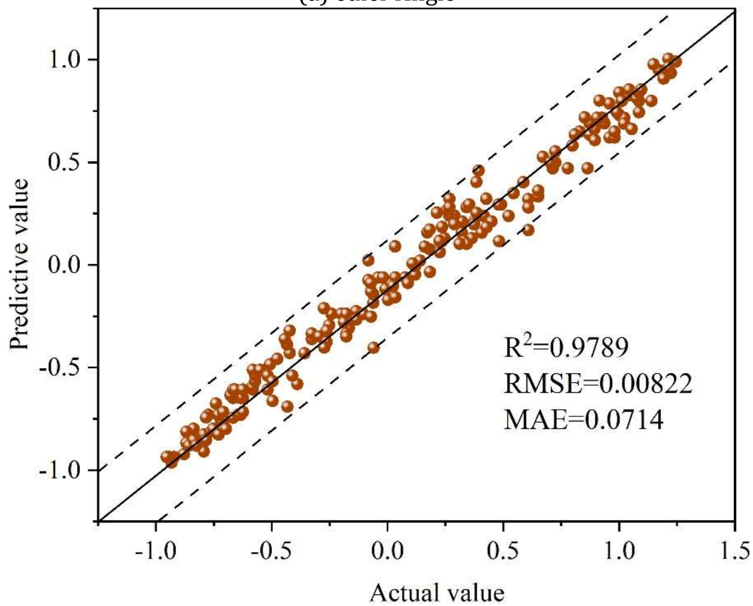

(b) shear strain

Fig. 5. The prediction results of the model and the measured results

5. Conclusion

In this paper, finite element technique is utilized to analyze the heat transfer of TiB2/Cu composites with different particle sizes and temperatures. The evolution of crystal plastic deformation of the metallurgical material is predicted using MEA-BP-FEA model based on finite elements. The results show that.

1) The correction factor for the simulated values of thermal conductivity of TiB2/Cu composites can be obtained using FEA. At 50~200℃, the simulated thermal conductivity of TiB2/Cu composites has a fluctuation of no more than 10% from the actual results, and after 200℃, the gap between the simulated thermal conductivity of composites and the actual results gradually decreases. And the thermal conductivity curves of the composites will be partially overlapped at 200℃.

2) The evaluation indexes of RMSE, MAE and R^2 of MEA-BP-FEA are significantly improved, which proves that the prediction model of MEA-BP-FEA guided by the crystalline plasticized finite element has accuracy and reliability.

References

[1] Tan, Z. Q., Zhang, Q., Guo, X. Y., Zhao, W. J., Zhou, C. S., & Liu, Y. (2020). New development of powder metallurgy in automotive industry. Journal of Central South University, 27(6), 1611-1623.

[2] Zaitsev, A. I. (2017). Prospective directions for development of metallurgy and materials science of steel. Pure and Applied Chemistry, 89(10), 1553-1565.

[3] Karaoğlu, S. Y., Karaoğlu, S., & Ünal, İ. (2021). Aerospace industry and aluminum metal matrix composites. International Journal of Aviation Science and Technology, 2(02), 73-81.

[4] Gohar, G. A., Manzoor, T., & Shah, A. N. (2018). Investigation of thermal and mechanical properties of Cu-Al alloys with silver addition prepared by powder metallurgy. Journal of Alloys and Compounds, 735, 802-812.

[5] Narayanasamy, P., Balaji, A. N., & Vettivel, S. C. (2018). Microstructural, electrical, thermal and tribological studies of copper-fly ash composites through powder metallurgy. Bulletin of the Polish Academy of Sciences Technical Sciences, 935-940.

[6] Zhao, Q., Sun, Q., Xin, S., Chen, Y., Wu, C., Wang, H., ... & Zhao, Y. (2022). High-strength titanium alloys for aerospace engineering applications: A review on melting-forging process. Materials Science and Engineering: A, 845, 143260.

[7] Wenga, T., Gwenzi, W., Jamro, I. A., & Ma, W. (2024). High-temperature corrosion-resistant alloy for waste-to-energy plants: Alloy designing, fabrication, and possible corrosion-resistance mechanism. Heliyon, 10(9).

[8] Wyatt, B. C., Nemani, S. K., Hilmas, G. E., Opila, E. J., & Anasori, B. (2024). Ultra-high temperature ceramics for extreme environments. Nature reviews materials, 9(11), 773-789.

[9] Ren, C., Enneti, R., & Ouyang, G. (2022). Refractory materials for corrosive or high-temperature environments. JOM, 74(11), 4305-4306.

[10] Zhang, A., & Li, Y. (2023). Thermal conductivity of aluminum alloys—a review. Materials, 16(8), 2972.

[11] Maj, J., Węglewski, W., Bochenek, K., Rogal, Ł., Woźniacka, S., & Basista, M. (2021). A comparative study of mechanical properties, thermal conductivity, residual stresses, and wear resistance of aluminum-alumina composites obtained by squeeze casting and powder metallurgy. Metallurgical and Materials Transactions A, 52(11), 4727-4736.

[12] Jenkins, T. P., Hess, C. F., Allison, S. W., & Eldridge, J. I. (2020). Measurements of turbine blade temperature in an operating aero engine using thermographic phosphors. Measurement Science and Technology, 31(4), 044003.

[13] Fang, G., Gao, X., & Song, Y. (2023). A review on ceramic matrix composites and environmental barrier coatings for aero-engine: Material development and failure analysis. Coatings, 13(2), 357.

[14] Sehgal, A. K., Juneja, C., Singh, J., & Kalsi, S. (2022). Comparative analysis and review of materials properties used in aerospace Industries: An overview. Materials Today: Proceedings, 48, 1609-1613.

[15] Nobrega, G., Cardoso, B., Souza, R., Pereira, J., Pontes, P., Catarino, S. O., ... & Moita, A. (2024). A review of novel heat transfer materials and fluids for aerospace applications. Aerospace, 11(4), 275.

[16] David Müzel, S., Bonhin, E. P., Guimarães, N. M., & Guidi, E. S. (2020). Application of the finite element method in the analysis of composite materials: A review. Polymers, 12(4), 818.

[17] Kim, H. S., Lim, Y. J., & Lee, H. L. (2020). Optimum location of outrigger in tall buildings using finite element analysis and gradient-based optimization method. Journal of Building Engineering, 31, 101379.

[18] Ji, H., & Li, D. (2021). A novel nonlinear finite element method for structural dynamic modeling of spacecraft under large deformation. Thin-Walled Structures, 165, 107926.

[19] Zhang, Y., Xu, H., Peng, R., Lu, Y., & Zhu, L. (2021). The state of the art of finite element analysis in mechanical clinching. International Journal of Precision Engineering and Manufacturing-Green Technology, 1-24.

[20] Wu, C. T., Wu, S. W., Niu, R. P., Jiang, C., & Liu, G. R. (2023). The polygonal finite element method for solving heat conduction problems. Engineering Analysis with Boundary Elements, 155, 935-947.

[21] Zhao Qiliang,Wang Lingmao,Yuan Linlin,Zhao Weijian,Watanabe Takahiko,Kawaguchi Tetsuo & Takeda Hitoshi. (2025) .Experimental Study and Multiscale Finite-Element Analysis on the Flexural Behavior of Precast Bridge Slabs with Headed Bar Joints. Journal of Bridge Engineering,30(5).

[22] Wang Fuzhang,Shah Faisal,Khan M. Ijaz,Alwetaishi Mamdooh,Malik M.Y. & Galal Ahmed M. (2022) .Insight into the relationship between the Fourier's law of heat conduction and Fick's law over a Riga device: Fourth grade analysis. Journal of the Indian Chemical Society,99(7).

[23] Liang Huiping,Yang Chunhua,Lv Mingjie,Zhang XuLong,Feng Zhenxiang,Li Yonggang & Sun Bei.

(2024) .Zinc roasting temperature field control with CFD model and reinforcement learning. Advanced Engineering Informatics,59,102332-.

[24] Hao Zhang,Xulong Cai,Peng Ni,Bowen Qin,Yuquan Ni,Zhiqiang Huang & Fubin Xin. (2025) .Prediction of coalbed methane content based on composite logging parameters and PCA-BP neural network. Journal of Applied Geophysics,236,105681-105681.

[25] Zhang Yudong,Tang Fan,Liang Xiaobin,Sun Jian,Li Hongxun & Ru Hang. (2023) .Prediction method of primary frequency modulation capability of power system based on MEA-BP algorithm. Energy Reports,9(S8),111-118.